# Ultrafast Phase Transformations in Metals Induced by Laser Irradiation: Molecular Dynamic Study

**Zhibin Lin* and Leonid Zhigilei****

*Department of Physics, **Department of Materials Science and Engineering, University of Virginia

## Introduction

Melting is a common physical phenomenon where solid-liquid phase transition occurs. Usually, melting starts at the free boundary where the energy barrier is low (or absent) for liquid to nucleate. The propagation of melting front, also called the heterogeneous melting, will typically take hundreds of picoseconds (ps) or longer, depending on the size of the melted region and the heating condition. Strong overheating induced by laser irradiation can significantly destabilize the crystal lattice and result in the nucleation of liquid phases inside the crystal, leading to the ultrafast homogeneous melting (~several ps) [1]. Using Molecular Dynamic (MD) method, we investigate the laser-induced phase transformations in metals (Au, Ni and Al) and compare with results of recent time-resolved diffraction experiments [1,2].

## Two Temperature Model (TTM)

In metals, laser energy is absorbed by conduction band electrons. Following the laser excitation, electrons quickly equilibrate among themselves (on the order of tens of femtoseconds (fs)) and slowly transfer the absorbed energy to the lattice through electron-phonon coupling. When laser pulse duration is much longer than the electron relaxation time, the electrons can be regarded to be at the local equilibrium described by the Fermi distribution with electron temperature $T_e$. The time evolution of the electron and lattice temperatures could then be described by two non-linear differential equations [3]:

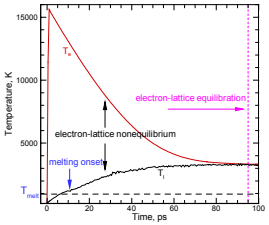


**Fig.1**. Time evolution of electron and lattice temperatures in 20 nm Au film irradiated by a 200 fs laser pulse at an absorbed fluence of 180 J/m$^2$

$$C_e(T_e)\frac{\partial T_e}{\partial t} = \nabla\left[K_e(T_e,T_l)\nabla T_e\right] - G(T_e)(T_e - T_l) + S(z,t)$$

$$C_l(T_l)\frac{\partial T_l}{\partial t} = \nabla\left[K_l(T_l)\nabla T_l\right] + G(T_e)(T_e - T_l) \quad \rightarrow \text{MD:} \quad m_i\frac{d^2\vec{r}_i}{dt^2} = \vec{F}_i + \xi m_i \vec{v}_i^{\,T} \quad [4]$$

where $C$ and $K$ are the heat capacities and thermal conductivities of the electrons and the lattice as denoted by subscripts $e$ and $l$, and $G$ is the electron-phonon coupling factor that characterizes the strength of the energy transfer rate. The Gaussian type source term $S(z,t)$ is used to describe the local laser energy deposition. In order to take into account phase transformation under strong non-equilibrium conditions, the second equation is substituted by MD, modified to account for the electron-lattice energy exchange [4].

## Molecular Dynamics (MD)

In this study, Newton's Equations of motion are solved for all particles in the system. MD computational cells consisting of 500,000 Au atoms and 864,000 Ni atoms are used in the simulations. Embedded Atom Method (EAM) potential is used to describe the interaction between atoms. Periodic boundary conditions are applied in two directions parallel to the free (001) surfaces.

Atomic configurations are obtained in MD simulations and are used for calculations of the pair density function $\rho(r)$ and pair correlation function $G(r)$ that provide direct information on the structural changes in the system [5]:

$$\rho(r) = \frac{1}{4\pi N r^2}\sum_{j=1}^{N}\sum_{i=1,i\neq j}^{N}\delta(r - r_{ij})$$

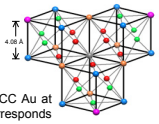


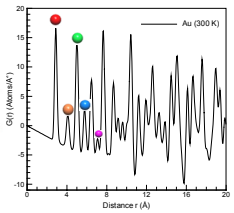


**Fig.2**. Pair correlation function $G(r)=4\pi r(\rho(r)-\rho_0)$ for FCC Au at 300 K. Atoms are colored coded so that each color corresponds to a particular distance to the central grey atom. For example, red corresponds to the first nearest neighbor in FCC.

## Atomic-level View of Ultrafast Melting

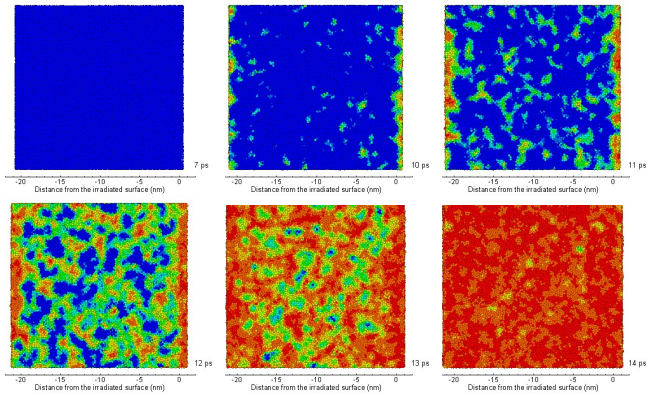


**Fig.3**. Snapshots of atomic configurations during the melting process as in Fig.1. Atoms are colored according to the local order parameter Φ - blue atoms have local crystalline surroundings, red atoms belong to the liquid phase. At 0 ps, the laser pulse is directed from the right to the left sides of the snapshots [6,7].

- Melting takes place within **~5 ps** while electron-lattice equilibration takes **~100 ps**.
- The relatively slow melting front propagation **cannot** compete with the fast homogeneous nucleation of numerous liquid regions inside the film when the overheating exceeds ~1.2-1.3$T_{melt}$.
- Before 7 ps, the gradual expansion of the film perpendicular to the free surfaces (**unixial lattice deformation**) facilitates the homogeneous melting by reducing the lattice stability. Also see the diffraction profiles in Fig.6.
- Current simulations are done for constant electron-phonon coupling $G_0$. Thermal excitation of 5d band electrons in Au could lead to the temperature dependence of the coupling constant, $G(T_e)$, and change $C_e(T_e)$. This results in significant changes in the timescales of the electron-lattice equilibration and melting [8].

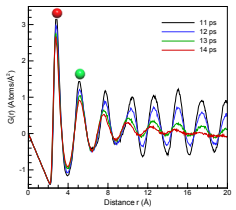


**Fig.4**. $G(r)$ during the homogeneous melting process as in Fig.1 [7].

## Loss of Long Range Order

- In Fig.4, peaks in the high $r$ region disappear, reflecting a complete loss of the long-range order.
- In Fig.5(b), the fast disappearance of the 2nd neighbor peak upon melting suggests that the interatomic distance responsible for this peak in the FCC structure is not characteristic of the short-range order in the liquid structure, where local tetrahedral and icosahedral short-range order dominates [9].

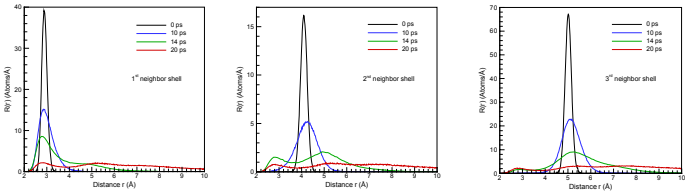


**Fig.5**. Radial distribution function $R(r)= 4\pi r^2\rho(r)$ for first three neighbor shells during the melting process as in Fig.1 [7].

## Diffraction Profiles

Diffraction profiles can be calculated from atomic configurations [5] and compared with results from time-resolved diffraction experiments [1].

$$S(Q) = 1 + \int_0^{\infty} 4\pi r^2 \rho(r)\frac{\sin(Qr)}{Qr}dr$$

- Three stages could be identified in the evolution of the diffraction profiles.
- First, up to ~4 ps, the reduction in diffraction peaks is due to the increasing thermal vibrations of atoms and can be well described by the Debye-Waller (DW) factor.
- Second, splitting and shift in the diffraction peaks in Fig.6(a) reflect the uniaxial lattice deformation along [001] direction leading to the following lattice transformation:

  **Cubic lattice → Tetragonal lattice**
- Finally, fast disappearance of diffraction peaks indicates the ultrafast solid-liquid transition, in agreement with diffraction experiments [1].

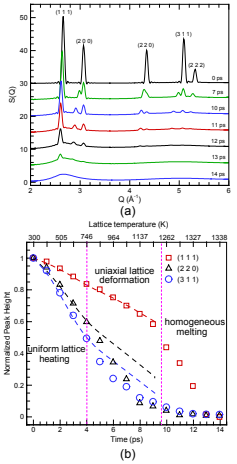


**Fig.6**. (a) Diffraction profiles during melting process as in Fig.1. (b) Normalized height of diffraction peaks as a function of time. All peak heights are normalized to their values at 0 ps (T=300 K). Dash lines are calculated through the DW factor at given lattice temperatures. The values of the average temperature of the film after the laser pulse are shown in the additional top x-axis [7].

## Generation of Coherent Acoustic Phonon in a Ni Film

- **Stronger** electron-phonon coupling in Ni (~10 times of Au) leads to the generation of compressive stresses.
- The relaxation of the compressive stresses results in the thermoelastic oscillations of the film [10].

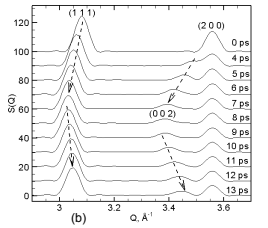


The oscillation period can be roughly estimated by 1D standing wave as $2L/v$, where $L$ is the film thickness and $v$ is the sound speed of ~5000 m/s for Ni.

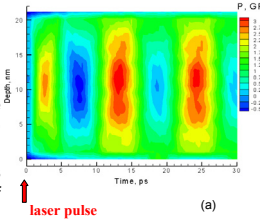


**Fig.7**. (a) Pressure contour plot of for 21 nm Ni film irradiated with a 200 fs laser pulse at an absorbed fluence of 100 J/m$^2$. (b) Diffraction profiles calculated for one period of thermoelastic oscillation of the film [10]. No melting occurs at this excitation level and the maximum lattice temperature rise is up to ~950 K. Our calculation results are consistent with recent experimental data for Al film [2].

## Conclusions

Results from MD simulations provide a direct link between the experimental observations in time-resolved diffraction experiments and atomic-level structural changes in the irradiated materials. Shift and splitting of the diffraction peaks reflect the thermoelastic and uniaxial lattice deformation of the film and can be used for experimental probing of the laser-induced ultrafast deformations. The observed differences in the evolution of the diffraction profiles in the homogeneous and heterogeneous melting processes can, along with kinetics arguments, be instrumental in distinguishing between the two melting mechanisms [7].

## References

[1] B.J. Siwick *et al. Science* **302**, 1382 (2003); K. Sokolowski-Tinten *et al. Nature* 422, 287 (2003); A.M. Lindenberg *et al. Science* **308**, 392 (2005)

[2] H. Park, X. Wang, S. Nie, R. Clinite, and J. Cao, *Phys. Rev. B* **72**, 100301 (2005)

[3] S.I. Anisimov, B.L. Kapeliovich, and T.L. Perel'man, *Sov. Phys. JETP* **39**, 375 (1974)

[4] D.S. Ivanov and L.V. Zhigilei, *Phys. Rev. B* **68**, 064114 (2003).

[5] T. Egami and S.J.L. Billinge, *Underneath the Bragg Peaks. Structural analysis of complex material*, Elsevier, (2003).

[6] Additional figures and movies can be found at *www.faculty.virginia.edu/CompMat/*

[7] Z. Lin and L.V. Zhigilei, *Phys. Rev. B* (in press)

[8] Z. Lin and L.V. Zhigilei, *Proceeding of SPIE: High Power Laser Ablation*, 2006 (in preparation)

[9] T. Schenk *et al. Phys. Rev. Lett.* **89**, 075507 (2002).

[10] Z. Lin, L.V. Zhigilei, *J. Phys.: Conf. Series* (in press)

## Acknowledgement

Z. Lin would like to gratefully acknowledge the introduction to the density correlation function analysis by Slava Kazmirov and Despina Louca. Financial support of this work is provided by the NSF through award CTS-0348503 and by the ONR through a sub-contract from the Electro-Optics Center, Penn State University.